

# Optimization of porous silicon multilayer as antireflection coatings for solar cells

E. Osorio<sup>a</sup>, R. Urteaga<sup>b,c</sup>, L. N. Acquaroli<sup>b</sup>, G. García-Salgado<sup>a</sup>, H. Juaréz<sup>a</sup> and R. R. Koropecski<sup>b,c</sup>

<sup>a</sup> Centro de Investigación en Dispositivos Semiconductores, Universidad Autónoma de Puebla CIDS-ICUAP, 14 sur and Av. San Claudio, San Manuel, 72570 Puebla, México

<sup>b</sup> Grupo de Semiconductores Nanoestructurados, Instituto de Desarrollo Tecnológico para la Industria Química (CONICET-UNL), Güemes 3450, 3000 Santa Fe, Argentina.

<sup>c</sup> Facultad de Ingeniería Química, UNL, Santiago del Estero 2829, 3000 Santa Fe, Argentina.

## Abstract

We present results of numerical simulation of optimized porous silicon (PS) multilayers used as antireflection coatings. For the simulations we introduce a figure of merit which has into account the transmittance of PS multilayers, the solar cell internal spectral response and the solar spectrum. Using a realistic range of porosities in the simulations (from 40% to 90%) we found an optimal three layers configuration which transfers to the cell 95.7% of the whole usable power. This value represents the 99.8% of the maximum attainable using the complete porosity range (from 0% to 100%). We fabricate the optimal PS three-layer, achieving a power transference to the substrate of 95.2%. In addition, taking advantage of the PS fabrication characteristics, we transferred a PS multilayer with specific optical response onto a crystalline silicon solar cell. This allows obtaining a tunable spectral response of the solar cell demonstrating the feasibility of transfer the porous antireflection coating onto any optical device.

Keywords: self-sustained porous silicon, optical properties, tuning spectral response, solar cell

## I. Introduction

The fabrication of crystalline silicon (c-Si) based solar cells (SCs) has been one of the most important topics of research since many decades, in order to take advantage of solar energy. Crystalline silicon reflects about 35% of the incident light within the spectral range of interest [1]. Many works have been devoted to improve this

1 performance by reducing the reflectance of c-Si based solar cells. The most effective  
2 way to reduce the reflectance is the use of antireflection coatings (ARC) and textured  
3 surfaces [1-4]. The most commonly used antireflection coating ARC for silicon solar  
4 cells is silicon nitride [5, 6] having a reported integrated reflection in the order of 10%.  
5  
6 The usual method for texturing the c-Si is by etching its surface with an alkaline  
7 solution such as NaOH or KOH. Etching of  $\langle 100 \rangle$  oriented wafers result in a pyramidal  
8 texture which is very efficient for reflection reduction purposes [2] giving an integrated  
9 reflectance of about 4% [3]. In the case of polycrystalline silicon, this method is not  
10 very effective since only a certain fraction of the c-Si grains have a  $\langle 100 \rangle$   
11 crystallographic orientation. Usually, different types of single [4-6] or multilayers [7-  
12 10] ARCs made of different materials are used to address the problem of low  
13 reflectance. Excellent broadband ARCs with reflectance less than 3% are obtainable  
14 today with a multilayered structure, such as  $\text{MgF}_2 / \text{Al}_2\text{O}_3 / \text{ZnS}$ , where each layer is  
15 separately deposited [10].  
16

17 The main disadvantages with the materials commonly used for coating are the  
18 requirement of multiple depositions, increasing the fabrication costs.  
19

20 Porous silicon (PS) appears as a low-cost production and an easy fabrication material to  
21 be used on c-Si SCs technology. In particular, the possibility of modulating the  
22 refractive index of PS layers in the fabrication process by modifying the current density,  
23 attract the attention of researchers to use it in SCs technology. Different authors have  
24 proposed to use PS as backside reflector [11], blue-to-red light transformer [12] and  
25 single or multilayer ARC [13-17].  
26

27 PS can be prepared by electrochemical anodization of crystalline silicon wafers in a  
28 fluorine-containing electrolyte [18]. The porosity of PS (i.e. the ratio between the void  
29  
30  
31  
32  
33  
34  
35  
36  
37  
38  
39  
40  
41  
42  
43  
44  
45  
46  
47  
48  
49  
50  
51  
52  
53  
54  
55  
56  
57  
58  
59  
60  
61  
62  
63  
64  
65

1 space volume and the total volume of the material), depends on preparation conditions  
2 such as current density and electrolyte composition. Provided the size of the PS  
3 structure is much smaller than the visible light wavelengths, PS behaves as an effective  
4 medium with a dielectric constant averaged between silicon, air and other components  
5 eventually adsorbed on the inner pore surfaces. An important feature of the PS  
6 preparation process is that a porosity in-depth profile can be built by using a current  
7 density time profile [19-21]. The anodization process is self-limited, which means that  
8 changing the current density within the fabrication process do not alter the already  
9 fabricated PS structure. This can be used to prepare PS multilayers and also to remove  
10 the porous layer from the c-Si substrate by using a high current pulse [19,21]. Then, the  
11 removed layer can be transferred to another substrate. This characteristic allows the  
12 fabrication of dielectric multilayers with specific optical response, which can be  
13 deposited onto a device to modify its spectral response; in particular, to make an ARC  
14 for a solar cell.

15  
16  
17  
18  
19  
20  
21  
22  
23  
24  
25  
26  
27  
28  
29  
30  
31  
32  
33  
34  
35  
36 Optimal PS-ARC on c-Si SCs produce an integrated reflectivity weighted with solar  
37 spectral irradiance of only 3% as reported elsewhere [15,16]. These studies on PS take  
38 into account only the reflection minimization of the ARCs coating. However, since the  
39 extinction coefficient of PS is not negligible, the total multilayer thickness must be  
40 optimized in order to prevent both reflection and absorption i.e., to maximize the power  
41 transmitted to the solar cell.

42  
43  
44  
45  
46  
47  
48  
49  
50  
51  
52  
53 In this work, we present numerical simulations results of optimum PS multilayers with  
54 different number of layers for SC ARC purposes. A systematic study was carried out to  
55 achieve an accurate determination of the effect of etching parameter variations in the PS  
56  
57  
58  
59  
60  
61  
62  
63  
64  
65

1 structure. In first place, a broad porosity span is required to reach the maximum  
2 refractive index range, toward an optimized PS ARC. The optimal ARC is then  
3  
4 designed, taking into account the transmittance of the PS multilayer, the solar spectrum  
5  
6 and the internal quantum efficiency of the solar cell.  
7  
8  
9

10  
11 In order to check the validity of the simulated results, a PS multilayer with a specific  
12 optical response (a microcavity) was fabricated and transferred onto a c-Si SC. The  
13 spectral response before and after the multilayer transference were measured and  
14 compared with results of simulations.  
15  
16  
17  
18  
19  
20  
21  
22

## 23 **II. Optimization of ARCs**

24  
25 The use of porous silicon as an antireflection coating consists in generating a series of  
26 dielectric layers as to maximize the transference of the incident light to the solar cell  
27 active device. The production of electric energy in a solar cell is determined by the  
28 spectral efficiency in combination with the spectrum of incident light. Thus, the  
29 dielectric layers must be designed to maximize the electrical output. This amount can be  
30 calculated as  
31  
32  
33  
34  
35  
36  
37  
38  
39  
40  
41

$$42 \quad P = \int_{\lambda_1}^{\lambda_2} T(\lambda) I_0(\lambda) \eta(\lambda) d\lambda, \quad (1)$$

43 where,  $I_0(\lambda)$  is the AM1.5 spectral irradiance,  $\eta(\lambda)$  refers to the internal efficiency of the  
44 solar cell [22] and  $T(\lambda)$  is the transmittance of the overall ARC stack. The transmittance  
45 of the multilayer as a function of wavelength was calculated using matrix formalism  
46 [23,24].  
47  
48  
49  
50  
51  
52

53 To calculate transmittance spectra, the complex refractive index and the physical  
54 thickness ( $d$ ) of each layer within the multilayer ARC are needed. Since pores and  
55  
56  
57  
58  
59  
60  
61  
62  
63  
64  
65

1 nanostructures size of PS are much smaller than incident wavelength, PS can be thought  
2 as a nanocomposite. Therefore, its optical properties can be modeled by using effective  
3 medium theories. In this work, we use the Looyenga-Landau-Lifshitz effective  
4 dielectric function [18], which is calculated from the porosity parameter ( $p$ ) and the  
5 dielectric functions of its components, silicon and air [25].  
6  
7  
8  
9  
10

11  
12  
13  
14 An appropriate parameter to evaluate the performance of the PS ARC stack can be  
15 defined as:  
16  
17

$$18 T_r = 100 \times \frac{\int_{\lambda_1}^{\lambda_2} T(\lambda) I_0(\lambda) \eta(\lambda) d\lambda}{\int_{\lambda_1}^{\lambda_2} I_0(\lambda) \eta(\lambda) d\lambda} . \quad (2)$$

19  
20  
21  
22  
23  
24 This parameter (hereafter called the transference parameter) gives a maximum value of  
25 100% for full transmittance of the multilayer, i.e., for a perfect ARC. In the case of a  
26 non-absorptive ARC,  $T=I-R$  where  $R$  stands for reflectance, and the maximization of  $T_r$   
27 is equivalent to the minimization of the weighted reflectance as is commonly  
28 implemented.  
29  
30  
31  
32  
33  
34  
35

36 The wavelength range in this work was chosen to be from  $\lambda_1 = 400$  to  $\lambda_2 = 1100$  nm.  
37 Typical c-Si solar cell efficiencies lie within this range. Besides, since the optical  
38 bandgap of c-Si (1.12 eV, about 1100 nm) widen this range to larger values of  
39 wavelength would be in vane. Moreover, the biggest amounts of energy that can be  
40 taken advantage from solar irradiance spectrum correspond to the chosen wavelength  
41 range, with a maximum at 500 nm. Therefore, in order to optimize Eq. (2), the solar cell  
42 and the solar irradiance spectra must be taken into account.  
43  
44  
45  
46  
47  
48  
49  
50  
51  
52  
53  
54  
55

56 The maximization was carried out using a computational code based on the simulated  
57 annealing and Nelder-Mead algorithms [26]. This codes starts from a given seed for the  
58  
59  
60  
61  
62  
63  
64  
65

1 optimization parameters (physical thicknesses and porosities of each layer) and iterates  
2 until a set of  $(d, p)$  maximizes Eq. (2) through the transmittance of the structure, for a  
3  
4 given angle of incidence. These iterations were performed for several numbers of layers  
5  
6 in the PS ARC multilayer.  
7

8  
9  
10  
11 The ARC system to optimize is modeled as an air/PS Multilayer/c-Si structure. The  
12  
13 incident light passes through (reflects and absorbs as well) the first medium (air), then  
14  
15 the PS multilayer ARC and finally the c-Si substrate.  
16  
17

18  
19  
20  
21 Simulated annealing and Nelder-Mead algorithms were used in a hybrid way, since the  
22  
23 results obtained by the first algorithm were used as seed in the latter.  
24  
25

26  
27  
28 In a first stage, we optimize Eq. (2) as described before using an ideal range of  
29  
30 porosities, i.e., from 0 to 100%, which in practice is a very hard task (if not impossible)  
31  
32 to reach. These calculations give a perspective of the best values of  $T_r$  that one can  
33  
34 expect for each PS ARC multilayer system.  
35  
36

37  
38  
39 Then, in order to optimize the ARC multilayer systems from realistic conditions, the  
40  
41 range of porosities was restricted to experimentally accessible fabrication parameters.  
42  
43 For our case, the lowest and highest experimental porosities available were limited to  
44  
45 40% and 90%, respectively.  
46  
47  
48  
49  
50

### 51 52 53 **III. Experimental**

#### 54 55 56 **III.a. Sample preparation**

57  
58  
59  
60  
61  
62  
63  
64  
65

1 PS layers were prepared by electrochemical anodization of heavily p-type boron doped  
2 c-Si wafers, with resistivity of  $2-4 \times 10^{-3} \Omega \cdot \text{cm}$ , (100) orientation, in a 1:2 (vol)  
3 electrolyte solution of HF (50%) and EtOH, respectively. The anodization cell is a  
4 Teflon<sup>®</sup> beaker where the c-Si wafer acts as the anode and the cathode is formed by a  
5 platinum wire [19-21].  
6

7  
8  
9  
10  
11 A computer controlled current source was used to fabricate PS multilayers from a given  
12 current density vs. time profile. Then, a 4 s electropolishing pulse of about  $230 \text{ mA/cm}^2$ ,  
13 in a 1:7 (vol) solution of HF (50%) and EtOH, was applied in order to separate the PS  
14 layers from c-Si substrates and transferred it onto the c-Si solar cell. After the  
15 electrochemical attacks, all the samples were rinsed with ethanol and dried under dry  $\text{N}_2$   
16 gas flow.  
17  
18  
19  
20  
21  
22  
23  
24  
25

26 The optical microcavity was fabricated following the procedure detailed in Ref. [21]. To  
27 prepare the multilayer, each layer of the structure we use two different current densities  
28 ( $64 \text{ mA/cm}^2$  and  $6 \text{ mA/cm}^2$ ) during 3 s and 39 s, respectively. Spectra were taken with  
29 an Ocean Optics HR4000 spectrometer at normal incidence to the substrate surface in  
30 the range 400 to 1100 nm.  
31  
32  
33  
34  
35  
36  
37  
38

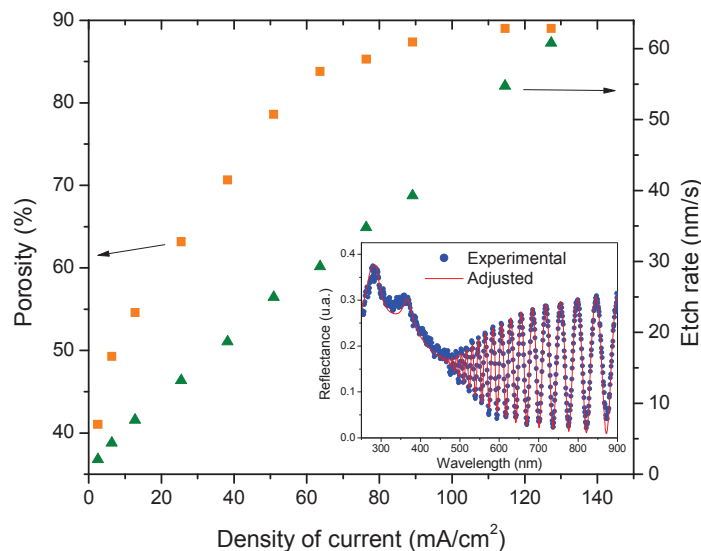
39 The c-Si solar cell used in this work was fabricated by CINVESTAV-MÉXICO.  
40  
41  
42

### 43 **III.b. Characterization of PS samples**

44 PS samples were characterized after fabrication by fitting their measured reflectance  
45 spectrum using a matrix method [23,24] and the effective medium approximation of  
46 Looyenga-Landau-Lifshitz [18]. From these fitting procedures the physical thicknesses  
47 and the porosities of the layers were acquired.  
48  
49  
50  
51  
52  
53  
54  
55  
56  
57  
58  
59  
60  
61  
62  
63  
64  
65

1 The lowest available porosity (40%) is assessed using a current density  $2.5 \text{ mA/cm}^2$ ,  
2 while the highest porosity (90%) is assessed using a current density of  $127 \text{ mA/cm}^2$ .  
3

4 Figure 1 shows the variation of the porosity and the etching rate with current density  
5 during formation of PS, as determinate by adjusting the experimental reflectance.  
6  
7  
8  
9



33  
34 **Fig. 1.** (Color online) Porosity (squares) and etch rate (triangles) vs. current density for electrochemical  
35 anodization conditions in the experiment. The porosity and thickness are obtained from the reflectance  
36 spectra at normal incidence (inset shows the spectra and fitted curve for  $3.06 \mu\text{m}$  thick layer fabricated  
37 with a density current of  $13 \text{ mA/cm}^2$ )  
38  
39  
40  
41  
42  
43

44 The spectral response of solar cells was measured using a chopped white light at 117 Hz  
45 coming from a halogen lamp, concentrated at the input of a monochromator and then  
46 focused alternatively on the sample and the calibrated cell. The photocurrent produced  
47 was detected and amplified by a Lock-in amplifier (synchronized to the frequency of the  
48 chopper) and derived to a PC for data processing. The measurement range was 400 to  
49 1100 nm.  
50  
51  
52  
53  
54  
55  
56  
57  
58  
59  
60  
61  
62  
63  
64  
65

#### IV. RESULTS AND DISCUSSIONS

From the maximization of  $T_r$  parameter (Eq.2) the thickness and porosity of each of layer in the ARC stack is obtained.

Figure 2 shows the  $T_r$  values obtained for dielectric different number of layers from 0 (without any ARC) to 7. In this Figure are shown the results obtained for both the ideal range of porosities (0 to 100%) and the realistic the range of porosities that can be experimentally accessible (40 to 90%).

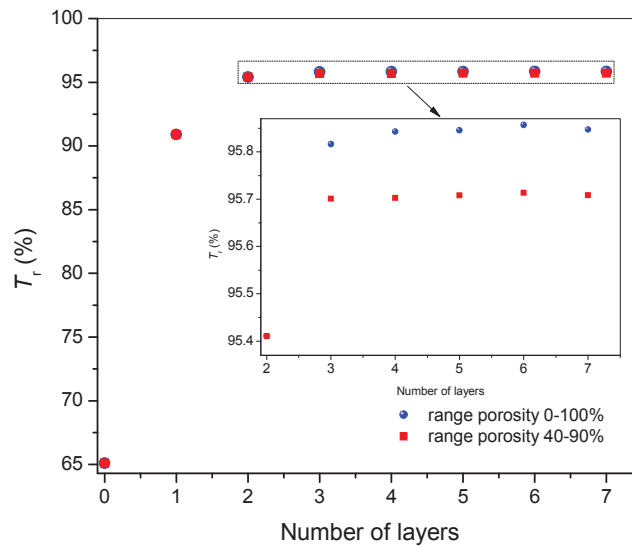


**Fig. 2.** (Color online) Optimum relative transmittance ( $T_r$  in Eq. (2)) for different number of dielectric layers. Two ranges of porosities are used in the calculations, an ideal 0-100% (dots) and 40-90% (squares). The inset shows a detail of the highest values of  $T_r$ .

It can be observed that  $T_r$  increase rapidly with the number of layers used, and reach a maximum at values close to 96% .The difference between the ideal and realistic range of porosities are lower than 0.2% in all cases.

1  
2  
3  
4  
5  
6  
7  
8  
9  
10  
11  
12  
13  
14  
15  
16  
17  
18  
19  
20  
21  
22  
23  
24  
25  
26  
27  
28  
29  
30  
31  
32  
33  
34  
35  
36  
37  
38  
39  
40  
41  
42  
43  
44  
45  
46  
47  
48  
49  
50  
51  
52  
53  
54  
55  
56  
57  
58  
59  
60  
61  
62  
63  
64  
65

Furthermore, for the realistic range of porosities, the increase in the  $T_r$  is negligible for a number of layers larger than three.

Figure 3 shows the values of total physical thickness ( $d_t$ ) obtained for the optimum layers obtained. As in Figure 1, the results for ideal and realistic range of porosities are shown.

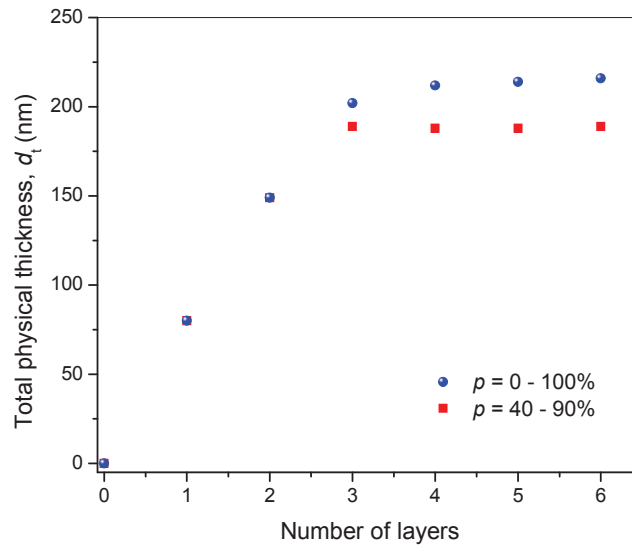
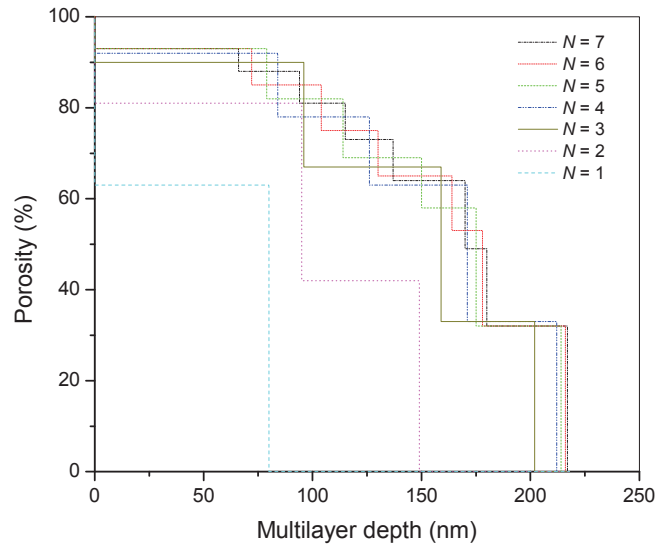


**Fig. 3.** (Color online) Total physical thickness ( $d_t$ ) using different number of dielectric layers. Two ranges of porosities are used in the calculations, an ideal 0-100% (dots) and 40-90% (squares).

It can be observed that  $d_t$  increase with the number of layers used. For the ideal range of porosities,  $d_t$  reach asymptotically a maximum at high number of layers. On the contrary, for the realistic range of porosities,  $d_t$  remains almost constant for  $N > 3$ .

The maximum in  $d_t$  value is the result of the balance between the lower reflectance that can be achieved when the intermediate region is larger and the increase of the absorbed light in the same region. This value is similar to the used empirically by other authors [17].

1  
2 Figure 4 shows the porosity profile obtained for different numbers of dielectric layers  
3  
4 when the ideal range of porosities is used.  
5  
6  
7  
8  
9



10  
11  
12  
13  
14  
15  
16  
17  
18  
19  
20  
21  
22  
23  
24  
25  
26  
27  
28  
29  
30  
31 **Fig. 4.** (Color online) Porosity profile obtained for different numbers of dielectric layers for the ideal  
32 porosity available range of 0% to 100%.  
33  
34  
35  
36

37 From this figure it is possible to observe that the profiles approach to a continuous curve  
38 when the number of layers increases. It can also be observed from this figure that the  
39 total thickness have an asymptotical behavior toward a value close to 220 nm.  
40  
41  
42  
43  
44  
45  
46

47 Figure 5 shows the profiles of porosities for different number of layers in the realistic  
48 case.  
49  
50  
51  
52  
53  
54  
55  
56  
57  
58  
59  
60  
61  
62  
63  
64  
65

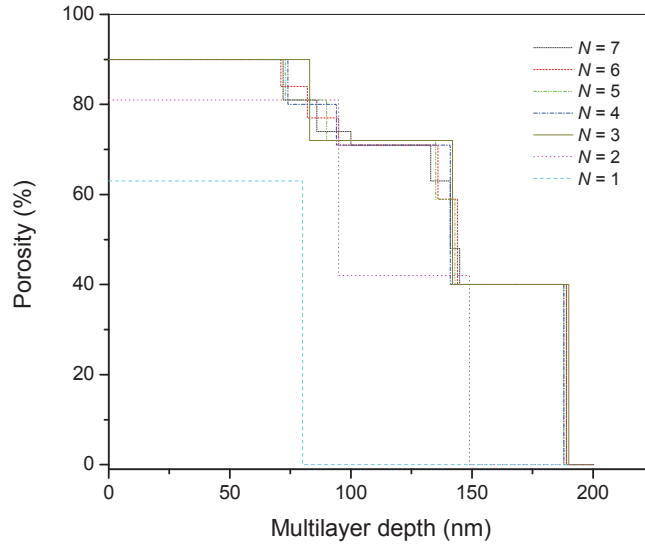


**Fig. 5.** (Color online) Porosity profile obtained for different numbers of dielectric layers when porosities range available is limited to 40% - 90%.

In this figure can be observed that the profile of porosities for  $N > 3$  reproduce with minor differences the profile for  $N = 3$ . These results indicates that the fabrication of porous silicon ARC with a number of layers more than three do not produces any substantial increase in  $T_r$  value.

Taking this into account, we fabricate a three layer PS ARC to evaluate his performance. Figure 6 shows the reflectance of the optimum porosity profile (Figure 4) and the fabricated multilayer of PS. We also include in the figure the best fit to the experimental data with a three layer configuration.

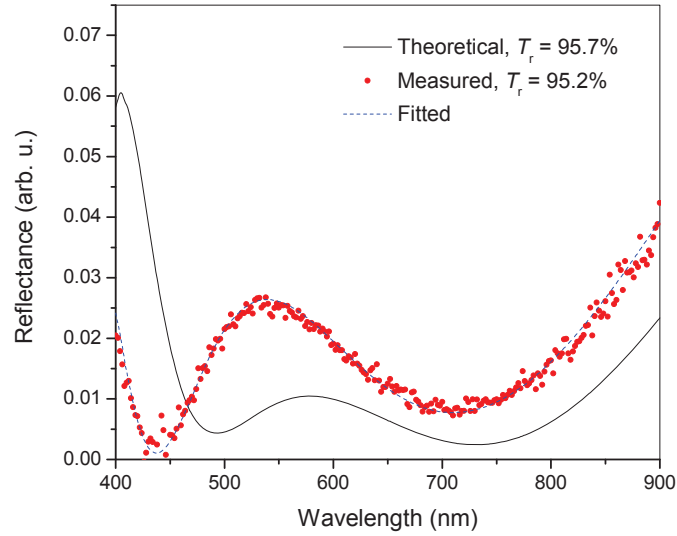


**Fig. 6.** (Color online) Experimental reflectance spectrum (dots) and adjusted spectrum (dashed line) of a three layer PS ARC. The optimum theoretical reflectance (line) is also included.

The experimental reflectance can be fitted accurately (see dashed line in Figure 6) with values of porosity and thickness for the tree layers given by [89, 70, 41] % and [77, 56, 39] nm, respectively.

The designed PS ARC has a transference parameter  $T_r$  of 95.2%, which is only 0.5% lower than maximum obtainable within the given restrictions in the porosity range, and 0.7 % lower than the maximum without restrictions.

This value is equivalent to a non-absorptive ARC with weighted reflectance of 4.8% that compares favorably with commercial single and double layer coatings [5,10,27,28].

In a first stage, we transferred the optimal 180 nm three-layer PS ARC onto a c-Si solar cell. However, since the thickness of this optimal layer is very thin, the transference process fails to cover the complete area of the solar cell, so external quantum efficiency could not measured. This is a technological problem that could be surely overcome.

1  
2 In order to demonstrate the feasibility of the transference method of PS ARC, we  
3  
4 fabricated a 2  $\mu\text{m}$  thick optical microcavity and deposited successfully onto a solar cell.  
5  
6 In this case, the entire surface of the SC was covered and the external quantum  
7  
8 efficiency of solar cell with and without microcavity was measured.  
9  
10

11  
12  
13  
14 Figure 7 show measured (dots) and fitting (line) reflectance spectra of the PS  
15  
16 microcavity transferred onto glass substrate at normal incidence. From the fitted curve  
17  
18 the values for thicknesses of the two different layers results 90 nm and 56 nm,  
19  
20 respectively, and their corresponding porosities of 80% and 49%, respectively.  
21  
22  
23

24  
25  
26 Figure 8 shows the external quantum efficiency (EQE) for the solar cell without  
27  
28 microcavity (dots) and with microcavity onto its surface (squares). From these two  
29  
30 measurements it can be observed that EQE of the solar cell copies the characteristics  
31  
32 shape of the optical microcavity spectral response.  
33  
34  
35

36  
37  
38 This result demonstrates that porous silicon fabrication techniques enable the possibility  
39  
40 to deposit porous multilayers onto any specific optical device in order to tune the  
41  
42 original spectral response of this device. It also should be noted that the porous layer  
43  
44 deposited onto the solar cell couples the features of its surface.  
45  
46  
47  
48  
49  
50  
51  
52  
53  
54  
55  
56  
57  
58  
59  
60  
61  
62  
63  
64  
65

1  
2  
3  
4  
5  
6  
7  
8  
9  
10  
11  
12  
13  
14  
15  
16  
17  
18  
19  
20  
21  
22  
23  
24  
25  
26  
27  
28  
29  
30  
31  
32  
33  
34  
35  
36  
37  
38  
39  
40  
41  
42  
43  
44  
45  
46  
47  
48  
49  
50  
51  
52  
53  
54  
55  
56  
57  
58  
59  
60  
61  
62  
63  
64  
65

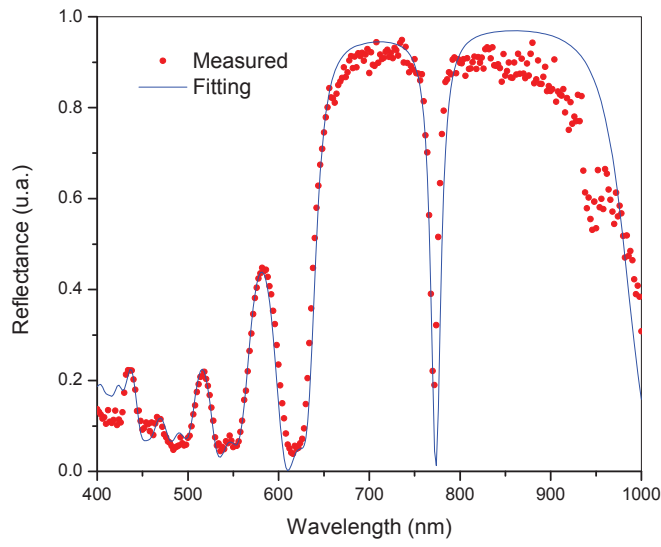


**Fig. 7.** (Color online) Measured (dots) and calculated (line) reflectance spectra of the PS microcavity onto glass substrate at normal incidence, obtained alternating two different current densities.

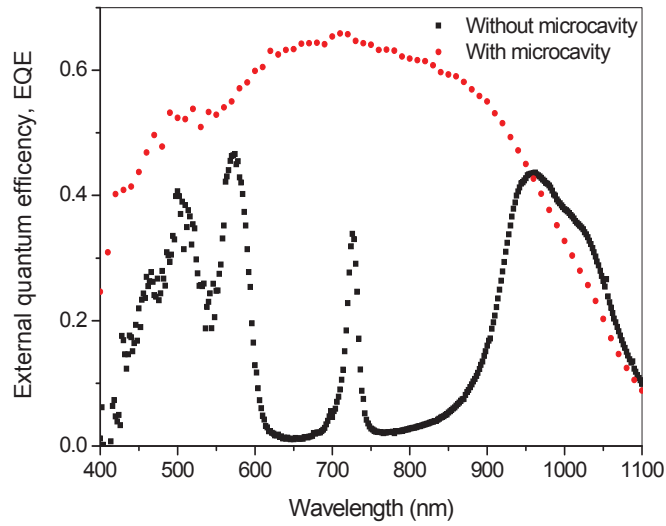


**Fig. 8.** (Color online) External quantum efficiency of the solar cell, without microcavity (dots) and with microcavity (squares).

## V. Conclusions

We made numerical simulations in order to optimize the performance of porous silicon antireflection coatings solar cells. Since the porous silicon has non zero absorbance, the optimization criterion was to maximize the energy transference to the cell structure instead of to minimize the weighted reflectance.

We found an optimal configuration with three layers that transmits 95.8% of the whole usable power to the active cell structure. We fabricate this optimal multilayer onto a crystalline silicon substrate obtaining up to 95.2% of energy transference to the silicon substrate. This value corresponds to a lost energy of 4.8% which is around a half of the corresponding to a conventional single layer ARC made of SiN.

We attempted to transfer the optimized 180 nm thick multilayer onto a solar cell. Although we did not succeed in cover all the cell area, we tested the validity of our simulations by transferring and measuring a thicker multilayer, with a sharp optical response. The measured energy resolved solar cell response presented features consistent with the spectral response of the used microcavity.

This result demonstrates the feasibility of the transference of a porous layer with specific spectral features to a device.

## References

- [1] B. M. Damiani, R. Lüdemann, D. S. Ruby, S. H. Zaidi, A. Rohatgi, Development of RIE-Textured silicon solar cells, Proc of the 28<sup>th</sup> IEEE Photovoltaic Specialists Conference, 15-22 September 2000, Anchorage, 371-374.
- [2] Kyunghae Kim, S.K. Dhungel, Sungwook Jung, D. Mangalaraj, J. Yi. Texturing of large area multi-crystalline silicon wafers through different chemical approaches for solar cell fabrication. Solar Energy Materials & Solar Cells **92** (2008) 960– 968.
- [3] J. Xiao, L. Wang, X. Li, X. Pi, D. Yang. Reflectivity of porous-pyramids structured silicon surface. Applied Surface Science **257** 472–475 (2010)

- 1  
2  
3  
4  
5  
6  
7  
8  
9  
10  
11  
12  
13  
14  
15  
16  
17  
18  
19  
20  
21  
22  
23  
24  
25  
26  
27  
28  
29  
30  
31  
32  
33  
34  
35  
36  
37  
38  
39  
40  
41  
42  
43  
44  
45  
46  
47  
48  
49  
50  
51  
52  
53  
54  
55  
56  
57  
58  
59  
60  
61  
62  
63  
64  
65
- [4] L.C.-K. Liao, C.-J. Huang, C.-C. Chen, C.-S. Huang, C.-T. Chen, S.-C. Lin, L.-C. Kuo. Process modeling and optimization of PECVD silicon nitride coated on silicon solar cell using neural networks. *Solar Energy Materials & Solar Cells* **71** (2002) 169–179.
- [5] R. Hezel and R. Schoerner. *J. Appl. Phys.* **52**, 3076 (1981).
- [6] A.G. Arberle. Over view on SiN surface passivation of crystalline Silicon solar cells. *Solar Energy Materials & Solar Cells* **65** (2001) 239-248.
- [7] Tadeusz Wiktorczyk, Michał Oles. Design, fabrication and optical characterization of cerium oxide-magnesium fluoride double layer antireflection coatings on monocrystalline silicon substrates. *Optical Materials* **29** (2007) 1768–1777.
- [8] S. E. Lee, S. W. Choi, J. Yi. Double-layer anti-reflection coating using MgF<sub>2</sub> and CeO<sub>2</sub> films on a crystalline silicon substrate. *Thin Solid Films* **376** (2000) 208-213.
- [9] M. Lipinski, A. Kaminski, J. F. Llzievre. Investigation of graded index SiO<sub>x</sub>N<sub>y</sub> antireflection coating for silicon solar cell manufacturing. *Phys Status Solidi C*, **4**(4): 1566 (2007).
- [10] D. Bouhafs, A. Moussi, A. Chikouche and J. M. Ruiz. Desing and simulation of antireflection coating systems for optoelectronic devices: Application to silicon solar cells. *Solar Energy Materials & Solar Cells*. **52**, 79 (1998).
- [11] J. Zettner, M. Thoenissen, Th. Hierl, R. Brendel, M. Schulz, *Prog. Photovolt. Res. Appl.* **6**, 423 (1998).
- [12] V.A. Skryshevsky, A. Laugier, V.I. Strikha, V.A. Vikulov, A. Kaninski, *Proc. 25th IEEE PVSC*, Wahington, p. 589 (1996).
- [13] W. J.Aziz, A. Ramizy,K. Ibrahim, Z. Hassan,K. Omar. The effect of anti-reflection coating of porous silicon on solar cells efficiency, *Optik-Int. J. Light Electron Opt*, (2011). doi:10.1016/j.ijleo.2010.08.025.
- [14] R J Martín-Palma, L Vázquez, J M Martínez-Duart, M Schnell and S. Schaefer. Antireflective porous-silicon coatings for multicrystalline solar cells: the effects of chemical etching and rapid thermal processing. *Semicond. Sci. Technol.* **16** (2001) 657–661.
- [15] S. Strehlke, S. Bastide, J. Guillet, C. Lévy-Clément. Design of porous silicon antireflection coatings for silicon solar Cells. *Materials Science and Engineering B* **69–70** (2000) 81–86.
- [16] M. Lipinski, P. Panek, E. Bel towska, H. Czternastek, Reduction of surface reflectivity by using double porous silicon layers. *Materials Science and Engineering B* **101** (2003) 297-299.

- 1  
2  
3  
4  
5  
6  
7  
8  
9  
10  
11  
12  
13  
14  
15  
16  
17  
18  
19  
20  
21  
22  
23  
24  
25  
26  
27  
28  
29  
30  
31  
32  
33  
34  
35  
36  
37  
38  
39  
40  
41  
42  
43  
44  
45  
46  
47  
48  
49  
50  
51  
52  
53  
54  
55  
56  
57  
58  
59  
60  
61  
62  
63  
64  
65
- [17] J. H. Selj, A. Thogersen, S. E. Foss and E. S. Marstein. Optimization of multilayer porous silicon antireflection coatings for silicon solar cells. *Journal of Applied Physics* **107**, 074904 (2010).
- [18] O. Bisi, Stefano Ossicini, L. Pavesi. Porous Silicon: a quantum sponge structure for silicon base optoelectronics. *Surface Science Reports* **38**, 1-126, (2000).
- [19]. L. N. Acquaroli, R. Urteaga, R. R Koropecski. Innovative design for optical porous silicon gas sensor. *Sensors and Actuators B: Chemical*. **149** (2010) 189–193.
- [20] L. N. Acquaroli, R. Urteaga, C. L. A. Berli, R. R Koropecski. Capillary filling in nanostructured porous silicon. *Langmuir* **27**(5), 2067 (2011).
- [21] R. Urteaga, O. Marín, L.N, Acquaroli, D. Comedi, J.A. Schmidt and R.R. Koropecski. Enhanced photoconductivity and fine response tuning in nanostructured porous silicon microcavities. *Journal of Physics: Conference Series* **167** (2009) 012005.
- [22] Yerokhov, V. Y. and Melnyk, I. I. *Renewable and Sustainable Energy Reviews* **3**, 291–322 (1999).
- [23] Pedrotti, F. L. and Pedrotti, L. S. *Introduction to Optics*. Prentice-Hall Inc, (1993).
- [24] Cisneros, J. I. *Ondas Electromagnéticas Fundamentos e aplicacoes*. Livro Texto (2000).
- [25] *Physical Properties and Data of Optical Materials (Optical Science and Engineering)*. Moriaki Wakaki, Keiei Kudo, Takehisa Shibuya. CRC. (2007). ISBN-10 / ASIN: 0824727614, ISBN-13 / EAN: 9780824727611.
- [26] W. H. Press, S. A. Teukolsky, W. T. Vetterling, B. P. Flannery. *Numerical Recipes - The Art of Scientific Computing*. 3rd. Ed. Cambridge University Press. New York. (2007).
- [27] K. L. Jiao and W. A. Anderson. *Solar Cells* **22**, 229\_(1987).
- [28] S. E. Lee, S. W. Choi, and J. Yi. *Thin Solid Films* **376**, 208 (2000).